Erschienen in: Physica Status Solidi (RRL) - Rapid Research Letters ; 10 (2016), 2. - S. 143-147
https://dx.doi.org/10.1002/pssr.201510334

Investigation of fill factor losses on 20.2% efficient n-type mono-like silicon solar cells with laser contact opening

Alexander Frey*, **Josh Engelhardt, Gabriel Micard, Giso Hahn, and Barbara Terheiden**

University of Konstanz, Department of Physics, 78457 Konstanz, Germany

Keywords crystalline silicon, boron emitters, laser contact opening, n-PERT

* Corresponding author: e-mail alexander.frey@uni-konstanz.de, Phone: +49 (0) 7531 88 2081, Fax: +49 (0) 7531 88 3895

Large area (243.36 cm^2) back-junction passivated emitter, rear totally diffused (PERT) solar cells with laser contact opening (LCO) on n-type *mono-like* crystalline Si with efficiencies of 20.2% are presented. Boron emitters with high electrical quality (implied open circuit voltage iV_{OC} up to 700 mV) are formed during a co-diffusion step using SiO_x:B layers. Increasing the rear metal contact coverage, we observed a decrease in fill factor (FF) instead of the expected increase due to the decrease of the back side series resistance. We show that it can be attributed to recombination centers (RCs) in the space charge region underneath the contact spots inducing an increasing second diode contribution. The presented empirical model for the RCs implemented in Synopsys Sentaurus TCAD allows for a successful reproduction of the FF, pseudo FF and V_{OC} behaviour with contact coverage. According to this model, the RCs induced by laser ablation and subsequently evaporation of Al have a shallow exponential distribution with a characteristic length of $L_T = 0.2$ μm and an effective surface density of $N^*_{T0} = 25$ cm^{-1}.

1 Introduction It is well known that n-type silicon as base material for solar cell technology has a higher efficiency potential compared to p-type Si thanks to lower capture cross-sections for holes of most common impurities in crystalline Si [1]. Around 40% of c-Si PV module manufacturing cost can be dedicated to the Si feedstock, crystal growth and wafering [2]. Therefore, potentially low-cost mono-like n-type Si from Bridgman technique using a seed crystal is of particular interest. The crystallographic quality of the mono-like ingots is comparable to Czochralski (Cz) grown silicon ingots when the solidification process is well controlled [3], enabling potentially low-cost fabrication of solar cells with high efficiencies.

It has been shown that dopant containing layers fabricated by chemical vapour deposition (CVD) can form an appropriate boron (B) diffusion source for n-type solar cell concepts [4–8] leading to high quality B emitters with low emitter saturation current density $j_{0e} < 50$ fA/cm^2 [6, 8]. With this method, only one high temperature step (co-diffusion) is necessary for emitter and back/front surface field (BSF/FSF) formation.

The industrial feasibility of this simplified and therefore time and potentially more cost effective method is demonstrated in this work on large area (243.36 cm^2) back-junction (BJ) passivated emitter, rear totally diffused (PERT) solar cells with laser contact opening (LCO) [9, 10] and evaporation of Al on n-type mono-like Si.

For contacting B emitters, screen-printing (SP) of Ag/Al H-grid is commonly used for industrially feasible bi-facial solar cells. However, this leads to open circuit voltage (V_{OC}) losses in the range of 30 mV [11] that could be attributed to metal spike formation penetrating the space charge region (SCR) [7].

As an alternative approach, LCO enables very small metallisation fractions and less metal spiking. The subsequent LCO metallisation can be realized by full area SP of Al pastes [12–14] or physical vapour deposition (PVD) of Al [12, 15], both resulting in low contact resistance that is

Konstanzer Online-Publikations-System (KOPS)
URL: http://nbn-resolving.de/urn:nbn:de:bsz:352-2-4yypec2534y1

much less dependent on the surface doping concentration. This allows usage of shallow B emitters with low j_{0e} and high implied V_{OC} (iV_{OC}). Therefore, these technologies lead potentially to high fill factor (FF) and V_{OC} values.

While SP of Al is an attractive low-cost industrially feasible process, which could remove potential laser damage underneath the contact spots, it may suffer from formation of voids during alloying [16, 17] affecting the series resistance and may also lead to shunt formation.

To avoid these potential drawbacks, we chose Al PVD for this study which, though less cost-effective, has been shown in [12] to lead to higher FF compared to full area SP of Al at comparable V_{OC} and metallization fraction. The potential of n-PERT cells using Al PVD was demonstrated by [15] reaching 22.5% efficiency with an advanced process sequence. A process sequence comparable to the one shown in this paper led to 21.3% efficiency using common BBr_3 emitters and an optimized metallization scheme [12].

However, if the LCO process is not completely optimized, the FF of solar cells using this technology can be lower than expected [18]. This was mainly attributed to an increased saturation current density of the second diode contribution (j_{02}) which is known to be induced by recombination centers (RCs) in the SCR.

Our aim is to investigate the influence of RCs, possibly induced by the LCO and subsequent evaporation of Al, on FF and V_{OC}. In this framework, we present an empirical model for the RC distribution underneath the contact spots that can successfully reproduce our measured FF and V_{OC} behaviour with coverage.

2 Experimental The schematic cross section of the n-PERT BJ solar cells with selective phosphorus (P) FSF is depicted in Fig. 1. Base resistivities of the n-type crystalline Si wafers are 6 Ω cm (mono-like) and 9 Ω cm (Cz-Si reference), respectively. After saw damage removal the wafers are single side alkaline textured.

After an industrial cleaning step (HCl-HF) the B-doped silicon oxide layer (SiO_x:B) is deposited in a single chamber inductively coupled plasma – plasma-enhanced chemical vapour deposition (ICP-PECVD) lab-tool. The reaction gases are SiH_4, CO_2 and B_2H_6:H. To form the B emitter and the P FSF in one high temperature diffusion step, the co-diffusion is carried out in a $POCl_3$ tube furnace in a two-step process similar to the one described in [5–7]. The deposition and diffusion parameters are optimized to achieve B emitters with low $j_{0e} < 50$ fA/cm^2 (comparable to $j_{0e} = 29.6$ fA/cm^2 published in [4]) and high iV_{OC} values up to 680 mV for mono-like Si and up to 700 mV for Cz-Si reference wafers (measured at 1 sun using a WCT-120 Sinton Lifetime tester on non metallised samples) which indicates the excellent electrical quality of the PECVD B emitters. Sheet resistances measured by a four point probe setup are in the range of 80–190 Ω/sq. Doping profiles measured by an electrochemical capacitance voltage (ECV) setup revealed depths of the emitters in the range of 465–520 nm with surface concentrations of 0.55–2.6×10^{19} cm^{-3}.

The selective FSF is fabricated by a selective emitter etch back (EEB) process [19]. The passivation of the FSF is realized by a dielectric layer stack of 7 nm thermal SiO_2 and 68 nm PECVD SiN_x, whereas the passivation of the B emitter is realized by a dielectric layer stack of 10 nm atomic layer deposited (ALD) Al_2O_3 and 120 nm PECVD SiN_x to obtain a sufficiently low j_{0e}.

Contact formation on the front side is realized by SP of commercially available Ag paste and firing in an IR belt furnace, whereas the rear side contact is formed by local laser ablation of the passivation layer stack and full area electron beam evaporation of Al. It has been proven that a picoseconds (ps) laser with photon energy higher than the silicon band gap can ablate Al_2O_3/SiN_x layer stacks without noticeable mechanical damage to the opened surface [10, 20]. We use a Gaussian laser beam with a pulse length of 10–15 ps and wavelength of 532 nm. The minimal laser fluence for sufficient ablation is of the order of 350 mJ/cm^2 [21]. For the fabrication of the n-PERT BJ solar cells a point structure (close-packed circles) with a contact diameter of 20 µm has been proven to be the optimal contact geometry in terms of series resistance and recombination losses [6]. The back side contact coverage is varied to investigate its influence on the solar cell characteristics for different B emitter profiles.

It has to be mentioned that, due to separate processing of each series, noticeable differences were measured in post process lifetime, j_{0e}, specific contact resistance (ρ_{BC}) and series resistance of the FSF ($R_{s,FSF}$) leading to their individual implementation in simulation for each series within a range given in the next section.

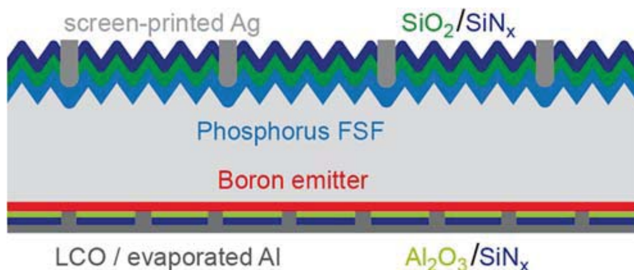

Figure 1 Schematic cross section of the n-PERT BJ solar cells with B emitter from ICP-PECV deposited BSG and selective phosphorus FSF. The contact formation is obtained via SP of Ag paste for the P-doped FSF and LCO and Al evaporation on the B-doped emitter. To obtain sufficient emitter passivation, an Al_2O_3/SiN_x stack is used.

3 Simulation The three-dimensional numerical simulation was performed using Synopsys TCAD Sentaurus. A base resistivity of 6 Ω cm and a minority carrier lifetime in the range of 525–700 µs were used. Measured ECV profiles for emitter and FSF were included with a surface recombination velocity of the B emitter surface of $s_{n0} = s_{p0}/10 = 25.8$ cm/s according to [22].

With fixed front side geometry, an arbitrary back side contact coverage (i.e. arbitrary distance between contact spots) is challenging to implement because of the difficulty of determining a (small) unit cell that can map the whole cell exactly by symmetry. To solve this issue, we implemented a simplified homogeneous front side geometry, thus having geometrical constraints only on the back side. Thus, the close-packed circular contacts are modelled by two quarters of contact at opposite corners of a square structure. A relationship between contact diameter d (20 µm for our case), contact coverage c and length/width of the unit cell a is given by

$$c = \pi/8 \cdot (d/a)^2 \, . \tag{1}$$

The FSF is fully covered by a contact with surface recombination velocity S_f that was adjusted to fit experimental j_{0e} data (average value including passivated and metallized areas: 80 fA/cm² to 110 fA/cm²). The front electrode associated to this contact has a series resistance $R_{s,front}$ defined by

$$R_{s,front} = R_{s,finger} + R_{s,FC} + R_{s,FSF} \, , \tag{2}$$

consisting of the series resistance of the finger ($R_{s,finger}$), of the front contact ($R_{s,FC}$) and of the FSF ($R_{s,FSF}$). Because the used geometry does not allow for the description of lateral carrier transport in the FSF which is the main contribution to the FSF series resistance, $R_{s,FSF}$ has to be calculated separately and added to $R_{s,front}$.

All contributions to $R_{s,front}$ were calculated from measurements leading to values in the range of 0.47–0.61 Ω cm².

The back electrode has a series resistance $R_{s,back}$ that depends on the specific contact resistance of the evaporated Al contacts ($\rho_{BC} = 2.5$–11.5×10^{-4} Ω cm² depending on B surface concentration) and of the coverage by the relation

$$R_{s,back} = \rho_{BC}/c \, . \tag{3}$$

Estimations of R_S at maximum power point were performed with the two light intensity method (TLIM) [23] from simulated IV curves at different light intensities. The 1 sun IV curve was then corrected for R_S allowing extracting the pseudo FF (pFF).

4 Modelling of recombination centers It is highly probable that the distribution of RCs (assumed to be located at midgap) is monotonously decreasing function with depth. We therefore chose an exponential decay following an empirical relationship

$$N_T^*(z) = N_{T0}^* \exp(-z/L_T) \, , \tag{4}$$

with the characteristic length of the distribution L_T, the effective surface density $N_{T0}^* = \sigma_e N_{T0}$, σ_e the capture cross section of the RCs and N_{T0} their surface density.

The RC distribution is chosen to be qualitatively consistent with the typical simulated local temperature distribution induced by a ps laser during dielectric layer ablation [20]. Adjusting it quantitatively to our measurement results (see Section 5) leads to $L_T = 0.2$ µm and $N_{T0}^* = 25$ cm^{-1}. This distribution has N_T^* values of 0.7 cm^{-1} to 2 cm^{-1} in the SCR which are comparable to values obtained in Al BSF ($N_T^* = 0.9$ cm^{-1} [24]).

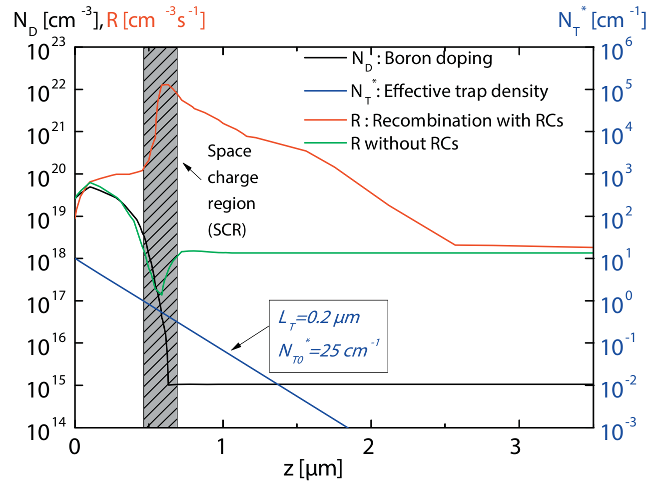

Figure 2 Simulation at maximum power point of the recombination activity R beneath the local contact with comparison to R outside the contact area showing additionally the RC distribution N_T^* and the doping profile N_D.

The simulation results in Fig. 2 show the impact of the RCs on recombination beneath the metal contact.

With RCs, we see that the recombination has a peak in the SCR corresponding to a minimum for the situation without RCs. This underlines the fact that a large j_{02} is induced by these RCs which mainly impacts the FF.

We observed also that recombination is slightly higher in the emitter (only slightly because Auger recombination is comparable with RCs recombination in this area) and much higher in the base below the SCR. While these contributions will impact the first diode and thus V_{OC}, the main contribution to the decrease in efficiency remains attributed to the RCs in the SCR inducing the j_{02} contribution.

5 Results In general, pFF reflects only the influence of recombination on FF (in the absence of shunt resistance), since the influence of R_s is removed completely.

Without RCs, the simulated pFF curves are almost flat (Fig. 3a) corresponding to a recombination activity almost independent of c. R_s is a decreasing function of the coverage because it is dominated by the emitter and contact resistance evolving with $1/c$ (see Eq. (3)) as confirmed by TLIM measurements. Therefore, FF should be an increasing function of c (Fig. 3b).

While this trend in FF fits to measurement data for low coverage ($c < 1\%$), the opposite trend is observed for higher coverage because of a decrease of the measured pFF with c in this range. This phenomenon can only be explained by an increasing recombination activity with c that is consistent with the presence of RCs under the contact

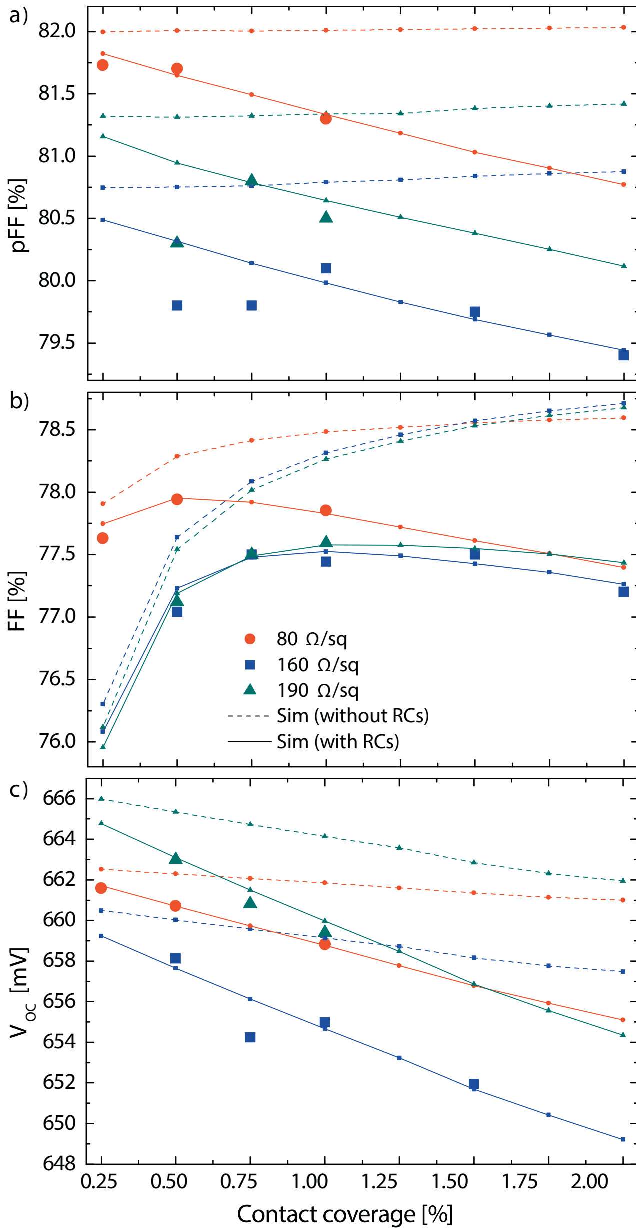

Figure 3 FF and V_{OC} determined by in-house measurements with a h.a.l.m flasher and pFF extracted from suns-V_{oc} measurements of the mono-like Si n-PERT BJ solar cells (large symbols) as well as results of the 3D simulations (small symbols: dashed lines without and solid lines with assumption of RCs underneath the local contact spots).

spots increasing locally recombination in emitter and base underneath as well as in SCR.

This pFF decrease is described by our model for RCs (Fig. 3a), allowing to match the measured FF accurately (Fig. 3b) for all emitters.

The increasing recombination activity with c also affects V_{OC} (Fig. 3c) and is very accurately fitted by our model confirming its consistency.

Considering the RCs, the optimal LCO contact coverage should be in the range of 0.5% to 1%, while higher efficiencies could be reached with higher coverage values without these RCs.

In Table 1 the results of the best large area (243.36 cm^2) n-PERT BJ solar cells with LCO are shown. The values were independently certified by ISE CalLab. The best mono-like cell (R_{SH} = 80 Ω/sq, c = 0.5%) exhibits an efficiency of 20.2% with V_{OC} of 661 mV (best Cz reference cell 20.5% with 672 mV for c = 1%).

The loss channels caused by the RCs underneath the local contact spots are as limiting as the loss channels introduced by using not optimized single SP H-grid, instead of high narrow fingers by e.g. print-on-print technology, photolithography and/or plating, leading to high R_S values and relatively high shadowing.

Table 1 Results of the best large area (243.36 cm^2) n-PERT BJ solar cells with LCO.

material	V_{OC} (mV)	J_{SC} (mA/cm^2)	FF (%)	η (%)	pFF (%)	R_s (Ω cm^2)
mono-like*	661.4	38.95	78.57	20.24	81.7	0.76
Cz ref*	672.3	39.14	77.95	20.51	81.2	0.77

* Independently certified by ISE CalLab.

6 Conclusions

In conclusion, large area (243.36 cm^2) PERT solar cells with an efficiency of 20.2% were presented in this work on potentially low-cost n-type mono-like Si (20.5% on Cz-Si reference cells). B emitter formation was realized by an industrially feasible co-diffusion step with ICP-PECV-deposited SiO_x:B doping layers. The origin of FF losses with increasing contact coverage could be explained by the presence of RCs induced by laser contact formation underneath the contact spots. Using an empirical model for their distribution, we have shown that the recombination they induce in the SCR and base region underneath allows for an accurate description of measured FF, but also V_{OC} losses. Because of these losses at higher contact coverage, only a narrow range of coverage values between 0.5–1.0% is optimal (for a spot size of 20 µm). Higher efficiencies and wider optimal coverage range can be expected without the detrimental influence of these RCs. While these defects can be partly attributed in our case to a not yet fully optimized laser process, they might not be completely avoidable even with an optimized process. Indeed, no such study has been performed so far to our knowledge and higher efficiencies reported in [15, 22] could be explained by a more advanced front metallization scheme.

Acknowledgements The authors would like to thank S. Gloger, F. Book, L. Mahlstädt, and B. Rettenmaier for their support. Part of this work was financially supported by the German Federal Ministry for the Environment, Nature Conservation and Nuclear Safety (FKZ 0325581) and within the project FKZ 0325449A via a subcontract granted by SolarWorld Innovations GmbH.

References

[1] D. Macdonald et al., Appl. Phys. Lett. **85**(18), 4061–4063 (2004).
[2] A. Goodrich et al., Sol. Energy Mater. Sol. Cells **114**, 110–135 (2013).
[3] N. Stoddard et al., Solid State Phenom. **131–133**, 1–8 (2008).
[4] R. Keding et al., Proc. 27th EU PVSEC, Frankfurt (2012).
[5] N. Wehmeier et al., Proc. 28th EU PVSEC, Paris (2013).
[6] J. Engelhardt et al., Energy Proc. **55**, 235–240 (2014).
[7] A. Frey et al., Proc. 29th EU PVSEC, Amsterdam (2014).
[8] J. Engelhardt et al., Appl. Phys. Lett. **107**, 042102 (2015).
[9] F. Haase et al., IEEE J. Photovolt.: Res. Appl. **3**, 976–984 (2013).
[10] J. Engelhardt et al., Energy Proc. **38**, 707–12 (2013).
[11] A. Edler et al., Progr. Photovolt.: Res. Appl. **23**(5), 620–627 (2014).
[12] V. Mertens et al., Proc. 28th EU PVSEC, Paris (2013).
[13] B. Lim et al., Proc. 29th EU PVSEC, Amsterdam (2014).
[14] W. Wang et al., IEEE J. Photovolt. **5**, 1245–1249 (2015).
[15] A. Urueña et al., Proc. 31st EU PVSEC, Hamburg (2015).
[16] E. Urrejola et al., Appl. Phys. Lett. **98**, 153508 (2011).
[17] R. Horbelt et al., Energy Proc. (2015) (in print).
[18] Y. Schiele et al., Proc. 42nd IEEE PVSC, New Orleans (2015).
[19] H. Haverkamp et al., Proc. 33rd IEEE PVSEC, San Diego (2008).
[20] A. Gurizzan and P. Villoresi, Eur. Phys. J. Plus **130**, 16 (2015).
[21] J. Engelhardt, Master thesis, University of Konstanz (2012)
[22] B. Hoex et al., Appl. Phys. Lett. **91**, 112107 (2007).
[23] G. Micard and G. Hahn, Proc. 28th EU PVSEC, Paris (2013).
[24] M. Rüdiger et al., J. Appl. Phys. **110**, 024508 (2011).